Supporting information

Rice husk-derived SiO_x/C composite for effective lithium-sulfur battery separator modification

Youngseul Cho[a,1], Se Hun Lee[b,1], Yongyeol Park[b,c], Tianyu Chen[a], Kyu Sang Lee[c], Ok Sung Jeon[b], Dongpyo Hong[b], Young Pyo Jeon[b], Young Joon Yoo[b,], Sang Yoon Park[d,*], Yuanzhe Piao[c,*]*

Corresponding authors:
Young Joon Yoo[b], Sang Yoon Park[d], and Yuanzhe Piao[c]

[a]Program in Nano Science and Technology, Graduate School of Convergence Science and Technology, Seoul National University, 145 Gwanggyo-ro, Yeongtong-gu, Suwon-Si, Gyeonggi-do 16229, Republic of Korea

[b]Center for Applied Electromagnetic Research for Advanced Institute of Convergence Technology, Seoul National University, Gyeonggi-do 16229, Republic of Korea

[c]Department of Applied Bioengineering, Graduate School of Convergence Science and Technology, Seoul National University, 145 Gwanggyo-ro, Yeongtong-gu, Suwon-Si, Gyeonggi-do 16229, Republic of Korea

[d]School of Electronic Engineering, Kyonggi University, Suwon-si, Republic of Korea

*Corresponding author e-mail addresses: youngjoonyoo@snu.ac.kr, yoonpark@kgu.ac.kr, parkat9@snu.ac.kr

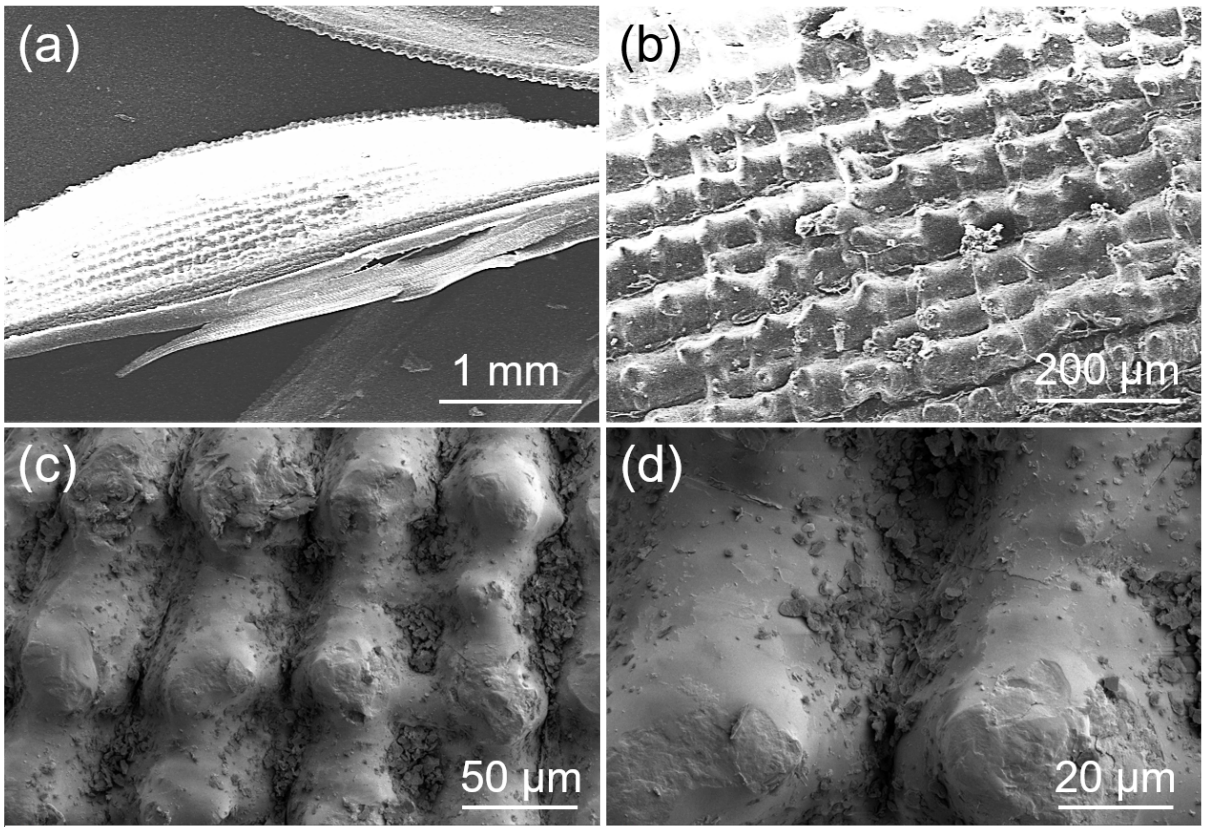

Fig. S1. SEM images of bare rice husk at (a-b) low magnification and (c-d) high magnification.

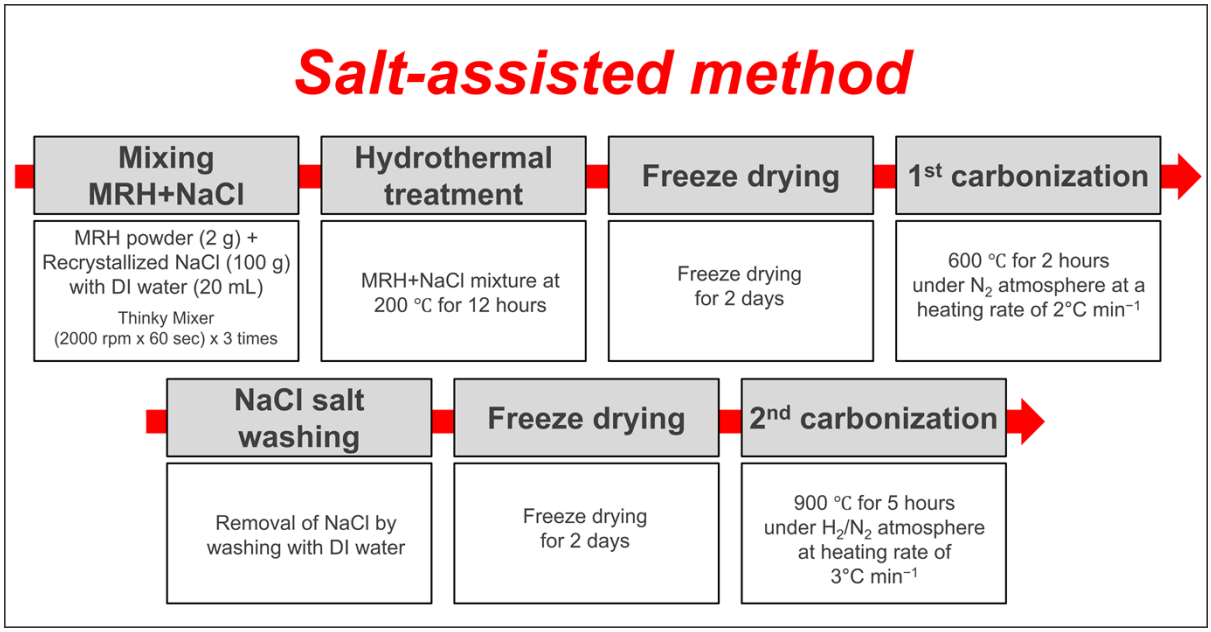

Fig. S2. Synthesis flow chart in the salt-assisted method.

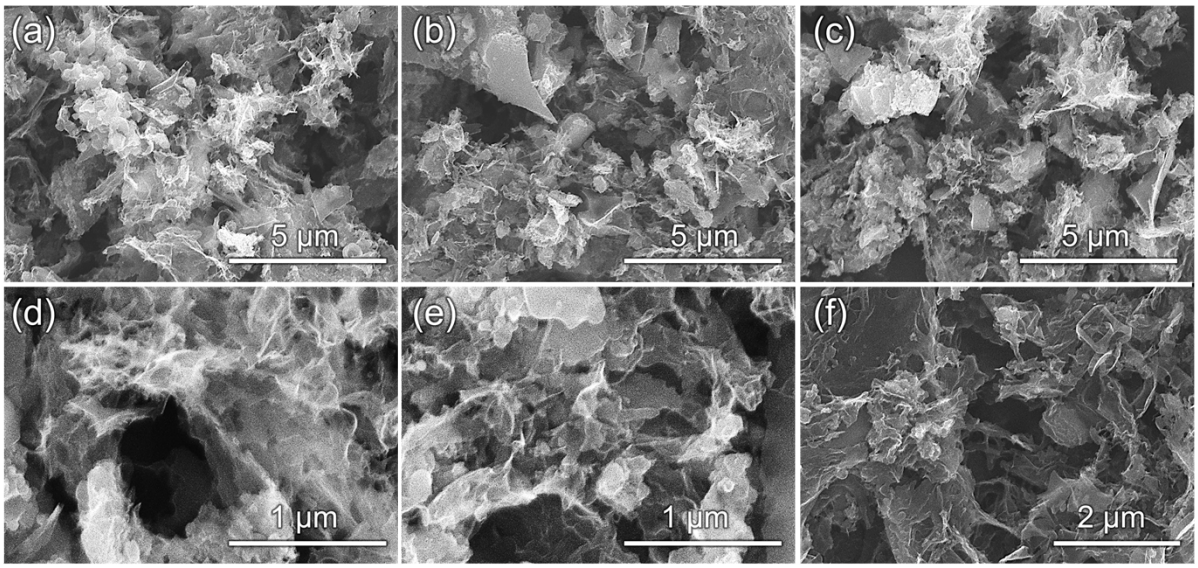

Fig. S3. SEM images of S-MRH with (a-c) low and (d-f) high magnifications.

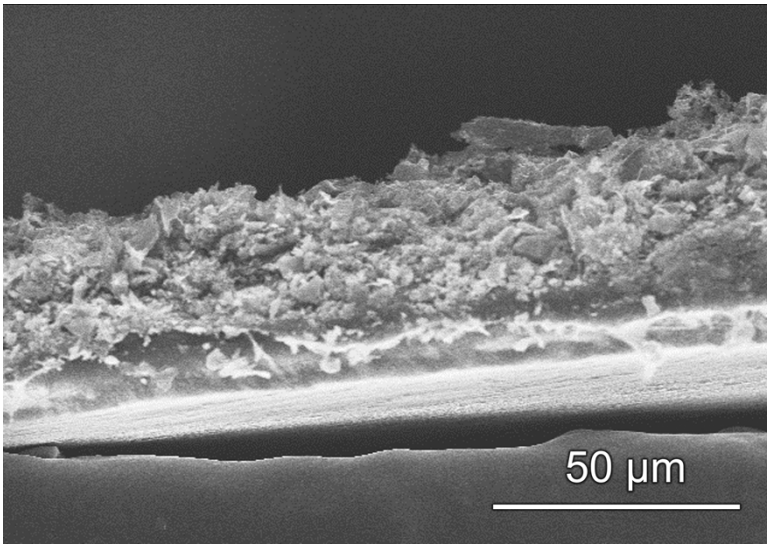

Fig. S4. Unclipped cross-sectional SEM image of S-MRH/PP.

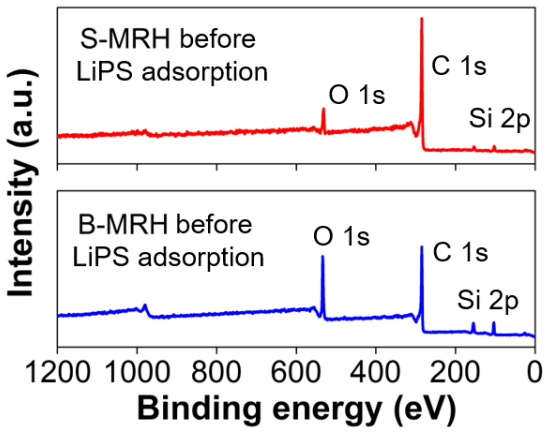

Fig. S5. XPS survey spectra of S-MRH and B-MRH before the lithium polysulfide adsorption test.

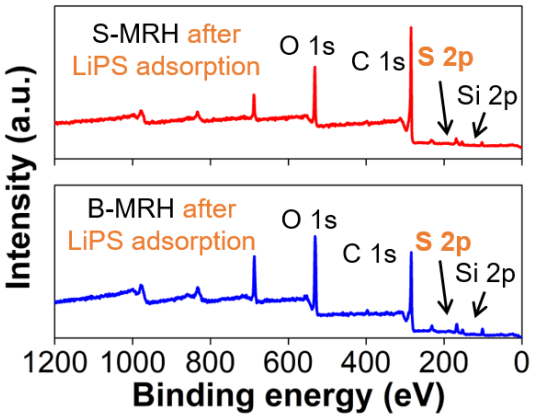

Fig. S6. XPS survey spectra of S-MRH and B-MRH after the lithium polysulfide adsorption test.

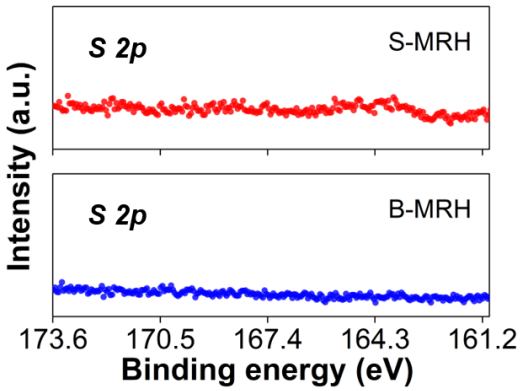

Fig. S7. S 2p XPS spectra of S-MRH and B-MRH before the lithium polysulfide adsorption test.

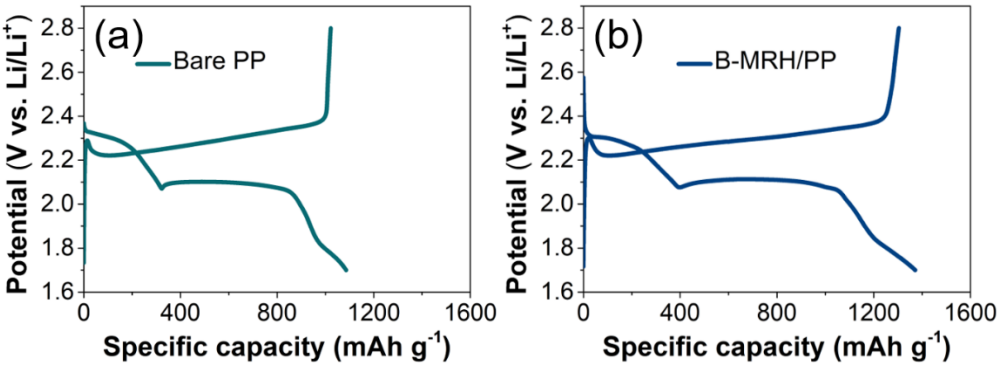

Fig. S8. Galvanostatic discharge and charge profiles of (a) Bare PP and (b) B-MRH/PP at 0.1C.

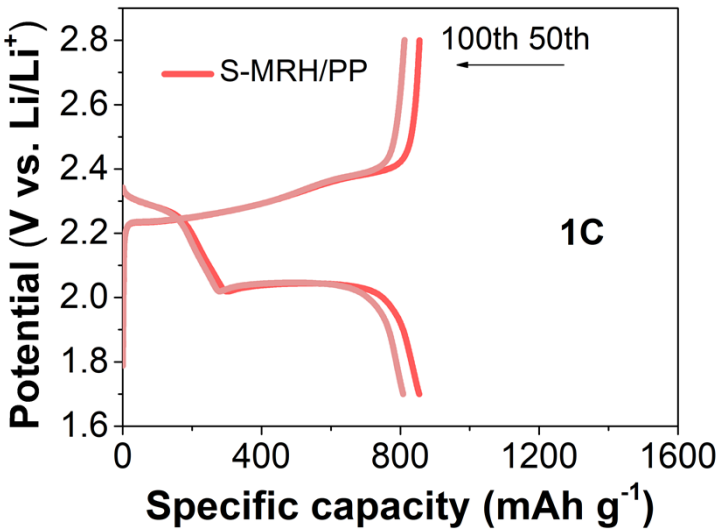

Fig. S9. Galvanostatic discharge and charge profiles of S-MRH/PP at 1C after 50th and 100th cycles in cycling test.

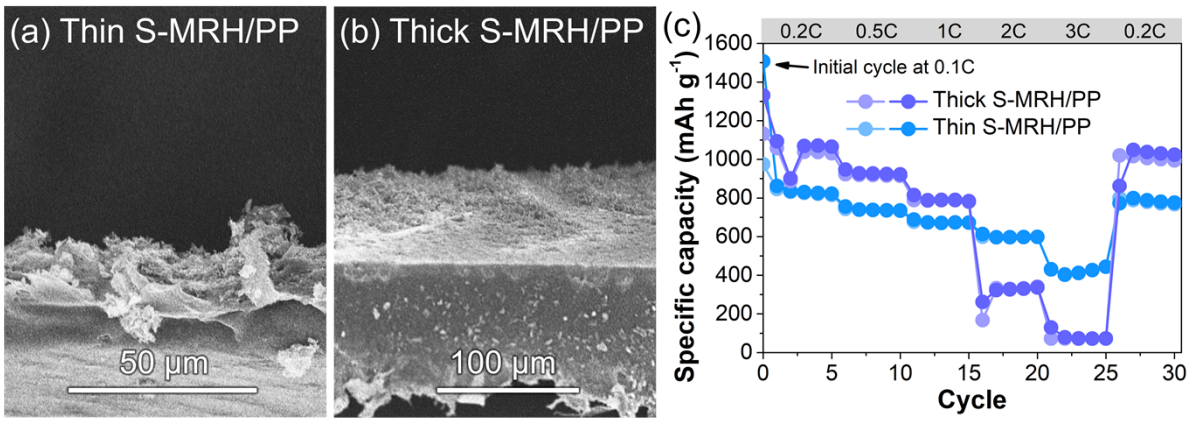

Fig. S10. Cross-sectional SEM images of (a) Thin S-MRH/PP and (b) Thick S-MRH/PP. (c) rate performance of Thin S-MRH/PP and Thick S-MRH/PP at various C-rates.

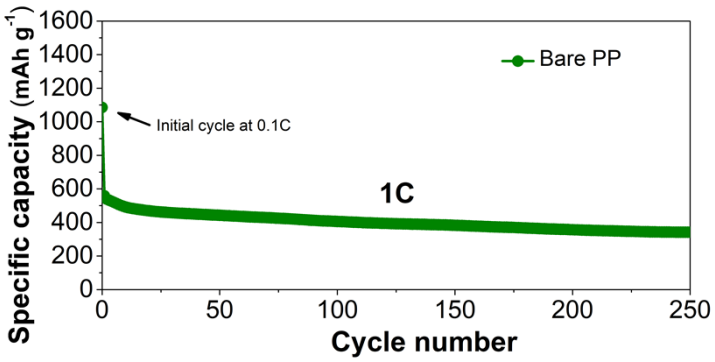

Fig. S11. Cycling performance of Bare PP electrode at 1C for 250 cycles.

- **The 2D progressive (2DP) and 2D instantaneous (2DI) nucleation and growth modes based on the Bewick, Fleischmann, and Thirsk (BFT) models:**

  For 2DI,
  $I/I_m = (t/t_m)\ \exp\{1/2[(1 - (t/t_m)^2]\}$

  For 2DP,
  $I/I_m = (t/t_m)^2\ \exp\{2/3[1 - (t/t_m)^3]\}$

- **The 3D progressive (3DP) and 3D instantaneous (3DI) nucleation and growth modes based on the Scharifker and Hills (SH) models:**

  For 3DI,
  $I/I_m = (1.9542\ t_m/t)^{1/2}\{1 - \exp[1.2564\ t/t_m]\}$

  For 3DP,
  $I/I_m = (1.2254\ t_m/t)^{1/2}\{1 - \exp[2.3367(t/t_m)^2]\}$

Fig. S12. The 2DP and 2DI nucleation and growth modes based on the BFT models and the 3DP and 3DI nucleation and growth modes based on the SH models.

- **Nucleation rate based on the 2D model:**

$$N_0 k_g^2 = \frac{\rho^2}{2\pi M^2 t_m^2}$$

M_{Li_2S} and ρ_{Li_2S} represent 46 g mol^{-1}, 1.66 g cm^{-3}, respectively.

Fig. S13. Nucleation rate calculation based on the 2D model.

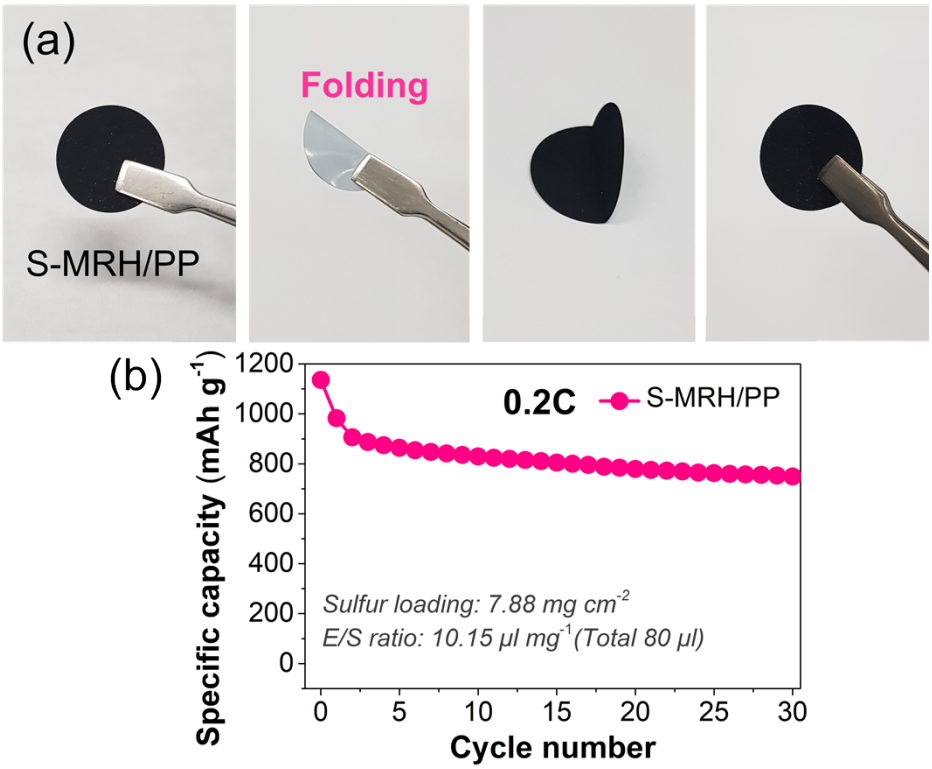

Fig. S14. (a) Digital photographs of folding test on S-MRH/PP. (b) Cycling performance of S-MRH/PP at 0.2 C for 30 cycles. The S-MRH/PP has been folded once as described in Fig. S14(a).

Table S1. Comparison chart illustrating the synthetic procedures and electrochemical performance of our study compared to other references, focusing on silicon oxide/carbon-based separator modifications or interlayers for Li-S batteries.

Sample	Synthetic procedure	Used chemicals	Rate performance	Cycle performance	References
Rice husk-derived SiO_x/porous carbon composite (S-MRH)	Salt-assisted method	Sodium chloride	Initial discharge capacity at 1444.9 mAh g^{-1} at 0.1C and 766.5 mAh g^{-1} at 3C (1.0 mg cm^{-2} sulfur loading)	Initial discharge capacity of 1414.4 mAh g^{-1} at 0.1C. After 60 cycles 987.27 mAh g^{-1} at 0.2C with capacity retention of 82.8% (sulfur loading of 4.0 mg cm^{-2} and lean electrolyte of 13.5 µl mg^{-1})	**This work**
Layered MWCNT/SiO_2/MWCNT membrane prepared via Langmuir-Blodgett sequential dip coating (LBSDC) and Langmuir-Blodgett (LBS)	Stöber synthetic technique for silica nanosphere	Ammonium hydroxide, tetraethyl orthosilicate (TEOS), MWCNT, and sodium dodecyl sulfate (SDS) surfactant	-	Initial discharge capacity of 1470 mAh g^{-1} at 0.5C. Capacity retention of 82% after 100 cycles at 0.5C (sulfur loading of 3.5 mg cm^{-2})	[S1]
UiO-66-NH_2@SiO_2-coated membrane	Metal-organic framework (MOF) synthesis for UIO-66-NH_2 on commercial silica	2-aminoterephthalic acid, silica, zirconium(IV) chloride, dimethylformamide (DMF), hydrochloric acid (HCl), and acetonitrile (ACN)	-	Initial discharge capacity of 1400 mAh g^{-1} at 0.1C (sulfur loading of 0.5 mg cm^{-2})	[S2]
Biomass-derived carbon fiber@SiO_2 composite (BCF@SiO_2)	Carbonization of absorbent cotton and silica	Cotton and silica solution	Initial discharge capacity of 1352.8 mAh g^{-1} at 0.1C. Reversible capacity of 628.6 mAh g^{-1} at 3C	Initial capacity of 963.2 mAh g-1 at 1C. After 500 cycles, 618.4 mAh g^{-1} with a capacity retention of 64.2% (sulfur loading of 4.2 mg cm^{-2})	[S3]
Nano-SiO_2 and MWCNT on aramid paper (SiO_2/AP)	Hot pressing treatment	Commercial SiO_2, para-aramid chopped fibers, MWCNT, sodium dodecyl benzenesulfonate (SDBS) solution,	Initial discharge capacity of 1635 mAh g^{-1} at 0.05C. Specific discharge capacity of 790 mAh g^{-1} at 3C	After 200 cycles, 1039 mAh g^{-1}	[S4]

		polyethylene oxide (PEO), sodium dodecyl sulfate (SDS), and anionic polyacrylamide (APAM)			
SiO_x-decorated stabilized polyacrylonitrile (sPAN-SiO_x) fiber mats	Electrospinning	Polyacrylonitrile (PAN), dimethylformamide (DMF), TEOS, and HCl	Discharge capacity of 531 mAh g^{-1} at 1C	Initial discharge capacity of 1321 mAh g^{-1} at C/5. After 100 cycles, 646 mAh g^{-1} at C/5 (sulfur loading of 3 mg cm^{-2})	[S5]
Silicon dioxide (SiO_2)−F co-doped poly-m-phenyleneisophthalamide (PMIA)	Electrospinning	m-phenylenediamine, isophthaloyl dichloride, N, N-Dimethylacetamide (DMAc), HCl, TEOS, and silane coupling agent 550 (KH550)	Discharge capacity of 686.6 mAh g^{-1} at 2C (sulfur loading of 2.1 mg cm^{-2} and electrolyte of 20 µl mg^{-2})	Initial discharge capacity of 1274.8 mAh g^{-1} at 0.5C. After 600 cycles, 814.8 mAh g^{-1} (sulfur loading of 2.1 mg cm^{-2} and electrolyte of 20 µl mg^{-2})	[S6]
Free-standing SiO_2/C composite nanofiber mat (FS-SiO_2/C-CNFM)	Electrospinning	TEOS, Polyvinylpyrrolidone(PVP), and nitric acid	Capacity of 504 mAh g^{-1} at 2C (sulfur loading of 1-1.6 mg cm^{-2})	Initial capacity of 1567 mAh g^{-1} at 0.1C (sulfur loading of 1-1.6 mg cm^{-2})	[S7]
SiO_2-nanotubes/carbon composite interlayer (SNTs@CP)	Template method	DL tartaric acid, TEOS, ammonia and CNT	Initial discharge capacity of 1031 mAh g^{-1} at 1C. Specific capacity of 585 mAh g^{-1} at 5C	Initial capacity of 1031 mAh g^{-1} at 1C. After 250 cycles, 810 mAh g^{-1} at 1C.	[S8]
SiO_2 hollow nanotubes-aramid fiber(SNTs-AP) interlayer	Template method and hot pressing	Para-aramid chopped fiber, para-aramid pulp fiber, sodium dodecylbenzene sulfonate (SDS), CNT, polyacrylamide (APAM), and DL tartaric acid.	Initial specific discharge capacity of 1220 mAh g^{-1} at 0.1C. Specific capacity of 808 mAh g^{-1} at 2C (sulfur loading of 1.53 mg cm^{-2} and electrolyte (1.5g sulfur, 50 µL of electrolyte))	Initial capacity of 1169 mAh g^{-1} at 0.2C. After 80 cycles, 1061 mAh g^{-1} at 0.2C (sulfur loading of 1.53 mg cm^{-2} and electrolyte (1.5g sulfur, 50 µL of electrolyte))	[S9]
Mesoporous Silica Nanosphere Composite Metal Cobalt-embedded in Nitrogen-Doped Carbon Nanotubes (Co-NCNTs/SiO_2)	Template method and co-impregnation method	Cyanoguanidine, $Co(NO_3)_2 \cdot 6H_2O$, CTAB, NAOH, and TEOS	Discharge capacity of 529.5 mAh g^{-1} at 2C	Initial capacity of 1239.8 mAh g^{-1} at 0.2C. After 100 cycles, 759.4 mAh g^{-1} at 0.2C with capacity retention of 61.2% (sulfur loading of 4 mg cm^{-2})	[S10]

References for Table S1

[1] M.S. Kim, L. Ma, S. Choudhury, S.S. Moganty, S. Wei, L.A. Archer, J. Mater. Chem. A, 4 (2016) 14709-14719.

[2] S. Suriyakumar, A.M. Stephan, N. Angulakshmi, M.H. Hassan, M.H. Alkordi, J. Mater. Chem. A, 6 (2018) 14623-14632.

[3] T. Liu, X.L. Sun, S.M. Sun, Q.H. Niu, H. Liu, W. Song, F.T. Cao, X.C. Li, T. Ohsaka, J.F. Wu, Electrochim. Acta, 295 (2019) 684-692.

[4] R. Li, X.G. Sun, J.Y. Zou, Q. He, Y.H. Xu, Mater. Res. Express, 6 (2019).

[5] E.C. Cengiz, A.A. Hamedani, S.H. Soytas, R. Demir-Cakan, Dalton Trans., 48 (2019) 4353-4361.

[6] N.P. Deng, E.B. Ticha, L.Y. Wang, Q.X. Li, H.J. Zhao, L. Gao, M. Liu, Y. Liu, W.M. Kang, B.W. Cheng, ChemElectroChem, 6 (2019) 4817-4830.

[7] A. Belgibayeva, I. Taniguchi, J. Power Sources, 484 (2021) 229308.

[8] C.B. Zhang, K. Li, J.T. Dai, X. Zhang, R. Li, J.Y. Zou, J. Alloy. Compd., 895 (2022) 162580.

[9] C.B. Zhang, K. Li, W. Luo, J.T. Dai, X. Zhang, R. Li, J.Y. Zou, Z.Y. Xu, Vacuum, 195 (2022) 110684.

[10] Y.M. Li, X.L. Bao, X.W. Wang, J.X. Zhao, P. Chen, H. Liu, H. Wang, L.S. Sun, W.Q. Liu, ACS Appl. Nano Mater., 6 (2023) 18780-18789.